Research Article | Vol. 26, No. 14 | 9 Jul 2018 | OPTICS EXPRESS A657
Optics EXPRESS

Using CDOM optical properties for estimating DOC concentrations and pCO_2 in the Lower Amazon River

ALINE DE MATOS VALERIO,[1,*] MILTON KAMPEL,[1] VINCENT VANTREPOTTE,[2] NICHOLAS D. WARD,[3] HENRIQUE OLIVEIRA SAWAKUCHI,[4,5] DIANI FERNANDA DA SILVA LESS,[6,7] VANIA NEU,[8] ALAN CUNHA,[6] AND JEFFREY RICHEY[9]

[1]*Instituto Nacional de Pesquisas Espaciais, INPE, 12227 010, São José dos Campos, SP, Brazil*
[2(c)]*entre National de la Recherche Scientifique, CNRS, USR3456, 97334 Cayenne, French Guyana*
[3]*Marine Science Laboratory, Pacific Northwest National Laboratory, Sequim, Washington, USA*
[4]*Universidade de São Paulo, USP/CENA, Caixa Postal 96, 13416 000, Piracicaba, SP, Brazil*
[5]*Department of Ecology and Environmental Science, Umeå University, SE, 901 87 Umeå, Sweden*
[6]*Universidade Federal do Amapá, UNIFAP, Caixa Postal 261, 68906 970, Macapá, AP, Brazil*
[7]*Universidade Federal do Oeste do Pará, UFOPA, 68040 050, Santarém-PA, Brazil*
[8]*Universidade Federal Rural da Amazônia, UFRA, Caixa Postal 917, 66077 530, Belém, PA, Brazil*
[9]*University of Washington, UW, 98195, Seattle, USA*
[*]*alineval@dsr.inpe.br*

Abstract: Coloured dissolved organic matter (CDOM) is one of the major contributors to the absorption budget of most freshwaters and can be used as a proxy to assess non-optical carbon fractions such as dissolved organic carbon (DOC) and the partial pressure of carbon dioxide (pCO_2). Nevertheless, riverine studies that explore the former relationships are still relatively scarce, especially within tropical regions. Here we document the spatial-seasonal variability of CDOM, DOC and pCO_2, and assess the potential of CDOM absorption coefficient ($a_{CDOM}(412)$) for estimating DOC concentration and pCO_2 along the Lower Amazon River. Our results revealed differences in the dissolved organic matter (DOM) quality between clearwater (CW) tributaries and the Amazon River mainstream. A linear relationship between DOC and CDOM was observed when tributaries and mainstream are evaluated separately (Amazon River: N = 42, R^2 = 0.74, p<0.05; CW: N = 13, R^2 = 0.57, p<0.05). However, this linear relationship was not observed during periods of higher rainfall and river discharge, requiring a specific model for these time periods to be developed (N = 25, R^2 = 0.58, p<0.05). A strong linear positive relation was found between $a_{CDOM}(412)$ and pCO_2(N = 69, R^2 = 0.65, p<0.05) along the lower river. pCO_2 was less affected by the optical difference between tributaries and mainstream waters or by the discharge conditions when compared to CDOM to DOC relationships. Including the river water temperature in the model improves our ability to estimate pCO_2 (N = 69; R^2 = 0.80, p<0.05). The ability to assess both DOC and pCO_2 from CDOM optical properties opens further perspectives on the use of ocean colour remote sensing data for monitoring carbon dynamics in large running water systems worldwide.

OCIS codes: (010.4450) Oceanic optics; (010.1690) Color; (010.1030) Absorption.

References and links

1. R. G. Wetzel and G. E. Likens, *Limnological Analyses* (Springer Science and Business Media, 2000).
2. T. J. Battin, L. A. Kaplan, S. Findlay, C. S. Hopkinson, E. Marti, A. I. Packman, J. D. Newbold, and F. Sabater, "Biophysical controls on organic carbon fluxes in fluvial networks," Nat. Geosci. **2**(8), 595 (2009).
3. N. D. Ward, T. S. Bianchi, P. M. Medeiros, M. Seidel, J. E. Richey, R. G. Keil, and H. O. Sawakuchi, "Where carbon goes when water flows: carbon cycling across the aquatic continuum," Front. Mater. Sci. **4**, 7 (2017).

#319302 https://doi.org/10.1364/OE.26.00A657
Journal © 2018 Received 12 Jan 2018; revised 26 Feb 2018; accepted 27 Feb 2018; published 31 May 2018

Optics EXPRESS

4. M. S. Johnson, J. Lehmann, E. C. Selva, M. Abdo, S. Riha, and E. G. Couto, "Organic carbon fluxes within and streamwater exports from headwater catchments in the southern Amazon," Hydrol. Processes **20**(12), 2599–2614 (2006).
5. N. D. Ward, H. O. Sawakuchi, V. Neu, D. F. S. Less, A. M. Valerio, A. C. Cunha, M. Kampel, T. S. Bianchi, A. V. Krusche, J. E. Richey, and R. G. Keil, "Velocity-amplified microbial respiration rates in the lower Amazon River," Limnol. Oceanogr. Lett., (in press).
6. B. Koehler, T. Landelius, G. A. Weyhenmeyer, N. Machida, and L. J. Tranvik, "Sunlight-induced carbon dioxide emissions from inland waters," Global Biogeochem. Cycles **28**(7), 696–711 (2014).
7. H. O. Sawakuchi, V. Neu, N. D. Ward, M. D. L. C. Barros, A. Valerio, W. Gagne-Maynard, A. C. Cunha, D. Fernanda, J. E. Diniz, D. C. Brito, A. V. Krusche, and J. E. Richey, "Carbon dioxide emissions along the lower Amazon River," Front. Mater. Sci. **4**, 1–12 (2017).
8. N. D. Ward, A. V. Krusche, H. O. Sawakuchi, D. C. Brito, A. C. Cunha, J. M. S. Moura, R. da Silva, P. L. Yager, R. G. Keil, and J. E. Richey, "The compositional evolution of dissolved and particulate organic matter along the lower Amazon River-Óbidos to the ocean," Mar. Chem. **177**, 244–256 (2015).
9. J. E. Richey, J. M. Melack, A. K. Aufdenkampe, V. M. Ballester, and L. L. Hess, "Outgassing from Amazonian rivers and wetlands as a large tropical source of atmospheric CO2," Nature **416**(6881), 617–620 (2002).
10. R. Lauerwald, G. Laruelle, J. Hartmann, P. Ciais, and P. A. G. Regnier, "Spatial patterns in CO2 evasion from the global river network," Global Biogeochem. Cycles **29**(5), 534 (2015).
11. G. Abril, J.-M. Martinez, L. F. Artigas, P. Moreira-Turcq, M. F. Benedetti, L. Vidal, T. Meziane, J.-H. Kim, M. C. Bernardes, N. Savoye, J. Deborde, E. L. Souza, P. Albéric, M. F. Landim de Souza, and F. Roland, "Amazon River carbon dioxide outgassing fuelled by wetlands," Nature **505**(7483), 395–398 (2014).
12. M. P. Curtarelli, I. Ogashawara, C. A. S. de Araújo, J. A. Lorenzzetti, J. A. D. Leão, E. Alcântara, and J. L. Stech, "Carbon dioxide emissions from Tucuruí reservoir (Amazon biome): New findings based on three-dimensional ecological model simulations," Sci. Total Environ. **551-552**, 676–694 (2016).
13. L. E. Vihermaa, S. Waldron, T. Domingues, J. Grace, E. G. Cosio, F. Limonchi, C. Hopkinson, H. R. da Rocha, and E. Gloor, "Fluvial carbon export from a lowland Amazonian rainforest in relation to atmospheric fluxes," J. Geophys. Res. Biogeosci. **121**, 3001 (2016).
14. P. Moreira-Turcq, M. P. Bonnet, M. Amorim, M. Bernardes, C. Lagane, L. Maurice, M. Perez, and P. Seyler, "Seasonal variability in concentration, composition, age, and fluxes of particulate organic carbon exchanged between the floodplain and Amazon River," Global Biogeochem. Cycles **27**(1), 119–130 (2013).
15. C. M. Rudorff, J. M. Melack, S. MacIntyre, C. C. F. Barbosa, and E. M. L. M. Novo, "Seasonal and spatial variability of CO2 emission from a large floodplain lake in the lower Amazon," J. Geophys. Res. Biogeosci. **116**, 1–12 (2011).
16. J. E. Richey, A. V. Krusche, M. S. Johnson, H. B. Da Cunha, and M. V. Ballester, "The role of rivers in the regional carbon balance," in *Amazonia and Global Change*, M. Keller, M. Bustamante, J. Gash and P. Silva Dias, eds. (American Geophysical Union, 2013).
17. V. Neu, C. Neill, and A. V. Krusche, "Gaseous and fluvial carbon export from an Amazon forest watershed," Biogeochemistry **105**(1-3), 133–147 (2011).
18. A. C. da Cunha and L. S. L. Sternberg, "Using stable isotopes 18 O and 2 H of lake water and biogeochemical analysis to identify factors affecting water quality in four estuarine Amazonian shallow lakes," Hydrol. Processes. (in press).
19. S. W. Correa, R. C. D. de Paiva, J. C. Espinoza, and W. Collischonn, "Multi-decadal Hydrological Retrospective: Case study of Amazon floods and droughts," J. Hydrol. (Amst.) **549**, 667 (2017).
20. J. C. Jiménez-Muñoz, C. Mattar, J. Barichivich, A. Santamaría-Artigas, K. Takahashi, Y. Malhi, J. A. Sobrino, and G. Schrier, "Record-breaking warming and extreme drought in the Amazon rainforest during the course of El Niño 2015-2016," Sci. Rep. **6**(1), 33130 (2016).
21. J. A. Marengo and J. C. Espinoza, "Extreme seasonal droughts and floods in Amazonia: Causes, trends and impacts," Int. J. Climatol. **36**(3), 1033–1050 (2016).
22. J. C. Espinoza, J. A. Marengo, J. Ronchail, J. M. Carpio, L. N. Flores, and J. L. Guyot, "The extreme 2014 flood in south-western Amazon basin: the role of tropical-subtropical South Atlantic SST gradient," Environ. Res. Lett. **9**(12), 124007 (2014).
23. N. D. Ward, R. G. Keil, P. M. Medeiros, D. C. Brito, A. C. Cunha, T. Dittmar, P. L. Yager, A. V. Krusche, and J. E. Richey, "Degradation of terrestrially derived macromolecules in the Amazon River," Nat. Geosci. **6**(7), 530–533 (2013).
24. P. L. Brezonik, L. G. Olmanson, J. C. Finlay, and M. E. Bauer, "Factors affecting the measurement of CDOM by remote sensing of optically complex inland waters," Remote Sens. Environ. **157**, 199–215 (2015).
25. V. Vantrepotte, F. P. Danhiez, H. Loisel, S. Ouillon, X. Mériaux, A. Cauvin, and D. Dessailly, "CDOM-DOC relationship in contrasted coastal waters: implication for DOC retrieval from ocean color remote sensing observation," Opt. Express **23**(1), 33–54 (2015).
26. C. G. Fichot and R. Benner, "The spectral slope coefficient of chromophoric dissolved organic matter (S275-295) as a tracer of terrigenous dissolved organic carbon in river-influenced ocean margins," Limnol. Oceanogr. **57**(5), 1453–1466 (2012).
27. R. G. M. Spencer, K. D. Butler, and G. R. Aiken, "Dissolved organic carbon and chromophoric dissolved organic matter properties of rivers in the USA," J. Geophys. Res. Biogeosci. **117**, G03001 (2012).

Optics EXPRESS

28. A. Mannino, M. E. Russ, and S. B. Hooker, "Algorithm development and validation for satellite-derived distributions of DOC and CDOM in the U.S. Middle Atlantic Bight," J. Geophys. Res. **113**(C7), C07051 (2008).
29. R. F. Chen and G. B. Gardner, "High-resolution measurements of chromophoric dissolved organic matter in the Mississippi and Atchafalaya River plume regions," Mar. Chem. **89**(1-4), 103–125 (2004).
30. A. Vodacek, N. V. Blough, M. D. DeGrandpre, M. D. DeGrandpre, and R. K. Nelson, "Seasonal variation of CDOM and DOC in the Middle Atlantic Bight: terrestrial inputs and photo oxidation," Limnol. Oceanogr. **42**(4), 674–686 (1997).
31. G. M. Ferrari, M. D. Dowell, S. Grossi, and C. Targa, "Relationship between the optical properties of chromophoric dissolved organic matter and total concentration of dissolved organic carbon in the southern Baltic Sea region," Mar. Chem. **55**(3-4), 299–316 (1996).
32. J. R. Helms, A. Stubbins, J. D. Ritchie, E. C. Minor, D. J. Kieber, and K. Mopper, "Absorption spectral slopes and slope ratios as indicators of molecular weight, source, and photobleaching of chromophoric dissolved organic matter," Limnol. Oceanogr. **53**(3), 955–969 (2008).
33. C. G. Fichot and R. Benner, "A novel method to estimate DOC concentrations from CDOM absorption coefficients in coastal waters," Geophys. Res. Lett. **38**(3), 1–5 (2011).
34. F. P. Danhiez, V. Vantrepotte, A. Cauvin, E. Lebourg, and H. Loisel, "Optical properties of chromophoric dissolved organic matter during a phytoplankton bloom. Implication for DOC estimates from CDOM absorption," Limnol. Oceanogr. **62**(4), 1409–1425 (2017).
35. N. B. Nelson and D. A. Siegel, "The global distribution and dynamics of chromophoric dissolved organic matter," Annu. Rev. Mar. Sci. **5**(1), 447–476 (2013).
36. J. F. Lapierre and P. A. Del Giorgio, "Geographical and environmental drivers of regional differences in the lake pCO2 versus DOC relationship across northern landscapes," J. Geophys. Res. Biogeosci. **117**, 1–10 (2012).
37. S. Larsen, T. Andersen, and D. O. Hessen, "The pCO2 in boreal lakes: Organic carbon as a universal predictor?" Global Biogeochem. Cycles **25**(2), 1–8 (2011).
38. S. Sobek, L. J. Tranvik, and J. J. Cole, "Temperature independence of carbon dioxide supersaturation in global lakes," Global Biogeochem. Cycles **19**(2), 1–10 (2005).
39. L. Pinho, C. M. Duarte, H. Marotta, and A. Enrich-Prast, "Temperature-dependence of the relationship between pCO2 and dissolved organic carbon in lakes," Biogeosciences Discuss. **12**(3), 2787–2808 (2015).
40. H. Marotta, C. M. Duarte, L. Pinho, and A. Enrich-Prast, "Rainfall leads to increased pCO2 in Brazilian coastal lakes," Biogeosciences **7**(5), 1607–1614 (2010).
41. T. Kutser, C. Verpoorter, B. Paavel, and L. J. Tranvik, "Estimating lake carbon fractions from remote sensing data," Remote Sens. Environ. **157**, 138–146 (2015).
42. S. E. Lohrenz and W. J. Cai, "Satellite ocean color assessment of air-sea fluxes of CO2 in a river-dominated coastal margin," Geophys. Res. Lett. **33**(1), L01601 (2006).
43. C. D. Clark, W. T. Hiscock, F. J. Millero, G. Hitchcock, L. Brand, W. L. Miller, L. Ziolkowski, R. F. Chen, and R. G. Zika, "CDOM distribution and CO2 production on the Southwest Florida Shelf," Mar. Chem. **89**(1-4), 145–167 (2004).
44. O. Nikiema, J. Devenon, and M. Baklouti, "Numerical modeling of the Amazon River plume," Cont. Shelf Res. **27**(7), 873–899 (2007).
45. H. Sioli, *The Amazon. Limnology and Landscape Ecology of a Mighty Tropical River and its Basin* (Springer Netherlands, 1984).
46. B. G. Mitchell, M. Kahru, J. Wieland, and M. Stramska, "Determination of spectral absorption coefficients of particles, dissolved material and phytoplankton for discrete water samples," in *Ocean Optics Protocols for Satellite Ocean Color Sensor Validation*, G. S. Fargion and J. L. Mueller, eds. (NASA Goddard Space Flight Center, 2003).
47. M. Babin, "Variations in the light absorption coefficients of phytoplankton, nonalgal particles, and dissolved organic matter in coastal waters around Europe," J. Geophys. Res. **108**(C7), 3211 (2003).
48. A. Bricaud, A. Morel, and L. Prieur, "Absorption by dissolved organic matter of the sea (yellow substance) in the UV and visible domains," Limnol. Oceanogr. **26**(1), 43–53 (1981).
49. H. O. Sawakuchi, D. Bastviken, A. O. Sawakuchi, N. D. Ward, C. D. Borges, S. M. Tsai, J. E. Richey, V. M. Ballester, and A. V. Krusche, "Oxidative mitigation of aquatic methane emissions in large Amazonian rivers," Glob. Change Biol. **1**, 1075 (2015).
50. T. Kutser, G. Casal Pascual, C. Barbosa, B. Paavel, R. Ferreira, L. Carvalho, and K. Toming, "Mapping inland water carbon content with Landsat 8 data," Int. J. Remote Sens. **37**(13), 2950–2961 (2016).
51. W. C. Gagne-Maynard, N. D. Ward, R. G. Keil, H. O. Sawakuchi, A. C. Da Cunha, V. Neu, D. C. Brito, D. F. Da Silva Less, J. E. M. Diniz, A. M. Valerio, M. Kampel, A. V. Krusche, and J. E. Richey, "Evaluation of primary production in the Lower Amazon River based on a dissolved oxygen stable isotopic mass balance," Front. Mater. Sci. **4**, 1–12 (2017).
52. M. Seidel, T. Dittmar, N. D. Ward, A. V. Krusche, J. E. Richey, P. L. Yager, and P. M. Medeiros, "Seasonal and spatial variability of dissolved organic matter composition in the lower Amazon River," Biogeochemistry **131**(3), 281–302 (2016).
53. R. Pereira, C. Isabella Bovolo, R. G. M. Spencer, P. J. Hernes, E. Tipping, A. Vieth-Hillebrand, N. Pedentchouk, N. A. Chappell, G. Parkin, and T. Wagner, "Mobilization of optically invisible dissolved organic matter in response to rainstorm events in a tropical forest headwater river," Geophys. Res. Lett. **41**(4), 1202–1208 (2014).

Optics EXPRESS

54. P. M. Medeiros, M. Seidel, N. D. Ward, E. J. Carpenter, H. R. Gomes, J. Niggemann, A. V. Krusche, J. E. Richey, P. L. Yager, and T. Dittmar, "Fate of the Amazon River dissolved organic matter in the tropical Atlantic Ocean," Global Biogeochem. Cycles **29**(5), 677 (2015).
55. M. Seidel, P. L. Yager, N. D. Ward, E. J. Carpenter, H. R. Gomes, A. V. Krusche, J. E. Richey, T. Dittmar, and P. M. Medeiros, "Molecular-level changes of dissolved organic matter along the Amazon River-to-ocean continuum," Mar. Chem. **177**, 218–231 (2015).
56. N. D. Ward, T. S. Bianchi, H. O. Sawakuchi, W. Gagne-Maynard, A. C. Cunha, D. C. Brito, V. Neu, A. M. Valerio, R. da Silva, A. V. Krusche, J. E. Richey, and R. G. Keil, "The reactivity of plant-derived organic matter and the potential importance of priming effects along the lower Amazon River," J. Geophys. Res. Biogeosci. **121**, 1–18 (2016).
57. T. S. Moore, M. D. Dowell, S. Bradt, and A. R. Verdu, "An optical water type framework for selecting and blending retrievals from bio-optical algorithms in lakes and coastal waters," Remote Sens. Environ. **143**, 97–111 (2014).
58. V. Vantrepotte, H. Loisel, D. Dessailly, and X. Meriaux, "Optical classification of contrasted coastal waters," Remote Sens. Environ. **123**, 306–323 (2012).
59. F. Mélin, V. Vantrepotte, M. Clerici, D. D'Alimonte, G. Zibordi, J. F. Berthon, and E. Canuti, "Multi-sensor satellite time series of optical properties and chlorophyll-a concentration in the Adriatic Sea," Prog. Oceanogr. **91**(3), 229–244 (2011).
60. H. Marotta, L. T. Paiva, and M. M. Petrucio, "Changes in thermal and oxygen stratification pattern coupled to CO2 outgassing persistence in two oligotrophic shallow lakes of the Atlantic Tropical Forest, Southeast Brazil," Limnology **10**(3), 195–202 (2009).
61. M. Fontes, H. Marotta, S. MacIntyre, and M. Petrucio, "Inter- and intra-annual variations of pCO2 and pO2 in a freshwater subtropical coastal lake," Inland Waters **5**(2), 107–116 (2015).
62. B. Hales, P. G. Strutton, M. Saraceno, R. Letelier, T. Takahashi, R. Feely, C. Sabine, and F. Chavez, "Satellite-based prediction of pCO2 in coastal waters of the eastern North Pacific," Prog. Oceanogr. **103**, 1–15 (2012).
63. Y. Zhu, S. Shang, W. Zhai, and M. Dai, "Satellite-derived surface water pCO2 and air-sea CO2 fluxes in the northern South China Sea in summer," Prog. Nat. Sci. **19**(6), 775–779 (2009).
64. Y. Bai, W.-J. Cai, X. He, W. Zhai, D. Pan, M. Dai, and P. Yu, "A mechanistic semi-analytical method for remotely sensing sea surface pCO2 in river-dominated coastal oceans: A case study from the East China Sea," J. Geophys. Res. Oceans **120**(3), 2331 (2015).
65. S. Kosten, F. Roland, D. M. L. Da Motta Marques, E. H. Van Nes, N. Mazzeo, L. D. S. L. Sternberg, M. Scheffer, and J. J. Cole, "Climate-dependent CO2 emissions from lakes," Global Biogeochem. Cycles **24**(2), 1–7 (2010).
66. A. Subramaniam, P. L. Yager, E. J. Carpenter, C. Mahaffey, K. Björkman, S. Cooley, A. B. Kustka, J. P. Montoya, S. A. Sañudo-Wilhelmy, R. Shipe, and D. G. Capone, "Amazon River enhances diazotrophy and carbon sequestration in the tropical North Atlantic Ocean," Proc. Natl. Acad. Sci. U.S.A. **105**(30), 10460–10465 (2008).
67. R. Weiss, "Carbon dioxide in water and seawater: the solubility of a non-ideal gas," Mar. Chem. **2**(3), 203–215 (1974).
68. E. E. Ellis, J. E. Richey, A. K. Aufdenkampe, A. V. Krusche, P. D. Quay, C. Salimon, and H. B. da Cunha, "Factors controlling water-column respiration in rivers of the central and southwestern Amazon Basin," Limnol. Oceanogr. **57**(2), 527–540 (2012).
69. D. Sun, C. Hu, Z. Qiu, J. P. Cannizzaro, and B. B. Barnes, "Influence of a red band-based water classification approach on chlorophyll algorithms for optically complex estuaries," Remote Sens. Environ. **155**, 289–302 (2014).
70. C. Le, C. Hu, J. Cannizzaro, D. English, F. Muller-Karger, and Z. Lee, "Evaluation of chlorophyll-a remote sensing algorithms for an optically complex estuary," Remote Sens. Environ. **129**, 75–89 (2013).
71. C. Le, Y. Li, Y. Zha, D. Sun, C. Huang, and H. Lu, "A four-band semi-analytical model for estimating chlorophyll a in highly turbid lakes: The case of Taihu Lake, China," Remote Sens. Environ. **113**, 1175 (2009).
72. A. A. Gitelson, G. Dall'Olmo, W. Moses, D. C. Rundquist, T. Barrow, T. R. Fisher, D. Gurlin, and J. Holz, "A simple semi-analytical model for remote estimation of chlorophyll-a in turbid waters: validation," Remote Sens. Environ. **112**(9), 3582–3593 (2008).
73. G. Dall'Olmo and A. A. Gitelson, "Effect of bio-optical parameter variability on the remote estimation of chlorophyll-a concentration in turbid productive waters: experimental results," Appl. Opt. **44**(3), 412–422 (2005).
74. K. Dörnhöfer and N. Oppelt, "Remote sensing for lake research and monitoring – Recent advances," Ecol. Indic. **64**, 105–122 (2016).
75. S. J. Dugdale, "A practitioner's guide to thermal infrared remote sensing of rivers and streams: recent advances, precautions and considerations," Wiley Interdiscip. Rev. Water **3**(2), 251–268 (2016).
76. R. N. Handcock, C. E. Torgersen, K. A. Cherkauer, A. R. Gillespie, K. Tockner, R. N. Faux, and J. Tan, "Thermal infrared remote sensing of water temperature in riverine landscapes," in *Fluvial Remote Sensing. Science and. Management*, P. E. Carbonneau and H. Piégay, eds (Wiley-Blackwell, 2012).
77. E. H. Alcântara, J. L. Stech, J. A. Lorenzzetti, M. P. Bonnet, X. Casamitjana, A. T. Assireu, and E. M. L. D. M. Novo, "Remote sensing of water surface temperature and heat flux over a tropical hydroelectric reservoir," Remote Sens. Environ. **114**(11), 2651–2665 (2010).

78. F. Cao, M. Tzortziou, C. Hu, A. Mannino, C. G. Fichot, R. Del Vecchio, R. G. Najjar, and M. Novak, "Remote sensing retrievals of colored dissolved organic matter and dissolved organic carbon dynamics in North American estuaries and their margins," Remote Sens. Environ. **205**, 151–165 (2018).

1. Introduction

Terrestrial humic substances are the dominant contributor to the dissolved organic matter pool (DOM) in freshwaters [1]. Dissolved organic carbon (DOC) is the major fraction of DOM active in the global carbon cycle, with fluvial export of DOC providing the largest flux of reduced carbon (0.25 Pg C y^{-1}) from land to ocean [2]. The fraction of DOM that absorbs ultraviolet (UV) and visible light, coloured dissolved organic matter (CDOM), is one of the major contributors to the absorption budget of most freshwaters. Freshwater systems also contain large amounts of carbon dioxide (CO_2) relative to the atmosphere [3]. In small streams most CO_2 is derived from soils and groundwater inputs [4], whereas in large riverine systems the input and in situ degradation of DOM by both microbes [5] and UV light [6] is a major source of CO_2, which is subsequently outgassed to the atmosphere.

The importance of freshwater systems on controlling the export and transformation of terrestrial DOM and the intimate relationship between these dynamics and the partial pressure of carbon dioxide (pCO_2) is well recognized [3,7–9]. However, we lack a detailed understanding of how these dynamics vary in space and time, particularly in the tropics, which contribute disproportionately to global CO_2 emissions and DOM export from inland waters [9,10]. The rivers in the Amazon basin, for example, are estimated to outgas from 0.5 to 1.39 Gt C yr^{-1} [7,11]. The dynamics of CDOM, DOC and pCO_2 in the Amazon River are largely influenced by the seasonal changes in the river discharge [8,9,12–15]. Seasonal variation in the rainfall intensity over the Amazon basin can also induce strong modulation in the quality (lability) of the DOC delivered to the river [4,16,17]. Several recent studies have emphasized trends towards the occurrence of extreme climatic events in some regions of the Amazon basin, illustrating the potential impact of such events on rain and river discharge patterns in the area [18–22].

Sawakuchi et al. [7] estimated that on the order of 0.48 Pg C $year^{-1}$ of CO_2 could be outgassed just from the lower Amazon River, if the entire spatial extent to the geographical mouth is considered, fueled primarily by the metabolism of DOM [5,23]. But the extreme heterogeneity and vast scales of the region make it difficult to interpolate over space and time, suggesting that suitable means of remote sensing could provide much-needed insight into the dynamics of this complex region. The objective of this work is to investigate the potential use of CDOM absorption for estimating DOC concentration and pCO_2 in the Lower Amazon River along a 900 km transect from the historic downstream gauging station, Óbidos, to the river mouth with samples collected in contrasting water types (clear and turbid waters) under different discharge conditions. This study provides the first bio-optical approach for assessing the carbon content at the Lower Amazon, a region recently pointed out as one of the most active CO_2 emission areas among inland waters [7].

Numerous studies have aimed to relate CDOM absorption properties (a_{CDOM}) to DOC content in estuarine and coastal waters [24–31] to use the latter optical proxy assessing DOC distribution through in situ or satellite observations. The latter studies have clearly emphasized the presence of highly significant linear relationships between a_{CDOM} and DOC in coastal waters dominated by terrestrial inputs of DOM, further illustrating the strong seasonal and regional dependency in the link between CDOM and organic carbon content. While CDOM absorption at a defined wavelength is providing quantitative information on DOM concentration, the spectral slope of the CDOM absorption spectra in the UV domain [275-295 nm] ($S_{275\text{-}295}$) has been shown to provide relevant insights into DOM composition and origin [26,32]. The potential of $S_{275\text{-}295}$ to be used as a relevant optical proxy of the DOC-normalized absorption coefficient of CDOM have been further demonstrated emphasizing the interest of this descriptor for better constraining the natural variability in the CDOM to DOC

relationship at both seasonal [33] and regional [25,34] scales. High $S_{275-295}$ values are usually related to highly (biologically or photochemically) degraded DOM [26,32,35]. Helms et al. [32] have further documented the interest of the ratio of two narrow spectral slopes (S_R; $S_{275-295}/S_{350-400}$) for assessing the molecular weight of the DOM within CDOM-rich waters.

Various potential descriptors of pCO_2 variability in inland ecosystems have been recently documented. A strong linear dependency between pCO_2 and DOC content has been for instance emphasized within diverse boreal and temperate inland waters [36–38]. The presence of such relationship in tropical regions was conversely not confirmed, including some Brazilian lakes of the Amazon basin [39,40]. CDOM, more likely adapted to the development of ocean colour remote sensing based pCO_2 inversion algorithms, has been also considered as a potential proxy of pCO_2 [41–43]. However, the potential of CDOM for estimating pCO_2 in the Amazon waters still need to be evaluated.

2. Materials and methods

2.1 Study area and sampling strategy

Six field campaigns were conducted to cover all hydrological seasons within the Lower Amazon River along a 900 km transect between the upstream boundary at Óbidos (01°55.141′ S, 55°31.543' W) and the Amazon River mouth (Fig. 1). The downstream boundary was the north and south channels near Macapá, which are the last two well-constrained channels near the Amazon River mouth (00°05.400′ S, 51°03.200′ W and 00°09.415′ S, 50°37.353 W, respectively). The region near the mouth is tidally influenced and experiences semi-diurnal flow reversals [8] but no saline intrusion is observed (Salinity 0) [44]. In addition to the mainstream Amazon River (Óbidos, Almeirim, Macapá stations, Fig. 1), samples were collected in all large tributaries within this section, including the Tapajos, Xingu, Paru, and Jari rivers, as well as the Lago Grande de Curuai floodplain lake. The lowland tributaries are classified as clearwater (CW) [45], with low turbidity and high levels of primary production when compared with the turbid water of the Amazon River and Lago Grande de Curuai [8].

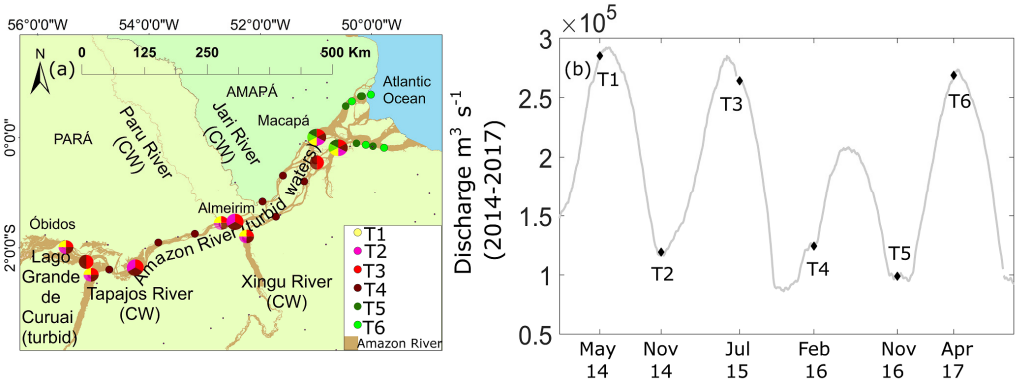

Fig. 1. a) Field campaigns (T stands for time of each campaign: T1-T6:); b) Seasonal discharge of the Amazon River during the studied period (2014-2017). Discharge data acquired from Óbidos Station (National Water Agency of Brazil, ANA).

CW rivers were sampled in May-14, Nov-14, Jul-15, Feb-16. During our two final cruises in low water (Nov-16) and high water (Apr-17) we pushed beyond our normal downstream boundary near Macapá to sample closer to the actual river mouth (Table 1, Fig. 1).

In practice, surface water (< 1m) was sampled in the frame of this study for assessing the concentration of the different variables of interest: CDOM, DOC, pCO_2 and chl-*a*. pCO_2, chl-*a* and temperature data are not available for T6.

Optics EXPRESS

The discharge of the Amazon River, which is a parameter translating the seasonal variability in the intensity of the inputs to the river from land-floodplain organic matter flush, was obtained from the National Water Agency of Brazil (ANA). The different in situ measurements performed in the frame of this study have allowed a description of the surface waters of the Lower Amazon River considering all possible discharge conditions over a 3-year period. Here we considered the first three months of the year representing the rising water season (Jan, Feb and Mar), followed by High (Apr, May, Jun), Falling (Jul, Aug, Sep) and Low (Oct, Nov, Dec) water seasons.

Table 1. Dates of sampling campaigns during the years of 2014-2017 and the respective season.

Campaign time ID	Discharge season	Date	Amazon River samples	Clearwater river samples
T1	High	May-14	yes	yes
T2	Low	Nov-14	yes	yes
T3	Falling	Jul-15	yes	yes
T4	Rising	Feb-16	yes	yes
T5	Low	Nov-16	yes	no
T6	High	April-17	yes	no

2.2 Methods

2.2.1 CDOM absorption

Surface water samples (N = 80) were first pre-filtered through 25 mm Whatman GF/F glass fiber filters (0.7 µm nominal pore size) to remove the larger part of the suspended matter. A second filtration was then performed on 0.2 µm polycarbonate membranes (Whatman nucleopore, 25 mm) under gentle vacuum (< 5 mm Hg) according to the NASA protocol for inherent optical properties [46]. Samples were stored in pre-combusted glass bottle (450°C, 6 hours) wrapped with aluminum foil and kept under refrigeration (4°C) until laboratory analysis. CDOM samples were put to room temperature before spectrophotometric analysis to avoid any bias due the thermal difference between the samples and the reference water (Milli-Q water). CDOM absorbance spectra were measured from 250 to 850 nm, using a Shimadzu, UV 2450 spectrophotometer with a 10-cm quartz cell. The CDOM absorption coefficient ($a_{CDOM}(\lambda)$) was calculated from absorbance measurements as followed (Eq. (1):

$$a_{CDOM} = 2.303 \cdot A(\lambda) / L \quad (1)$$

where A(λ) is the absorbance of the filtered water sample at the specific wavelength λ and L is the optical pathway of the quartz cell in meters (here 0.1 m).

As recommended by Babin et al. [47] in coastal and estuarine waters, a baseline correction was performed to each spectrum by subtracting the mean absorbance in the range of 680-690 nm from the whole spectrum. The absorption spectral shape of CDOM is estimated using a linear least-squares regression of the logarithm of $a_{CDOM}(\lambda)$ and reported with units of nm^{-1} [48] (Eq. (2):

$$a_{CDOM}(\lambda) = a_{CDOM}(\lambda_0) e^{-S(\lambda-\lambda_0)} \quad (2)$$

where $a_{CDOM}(\lambda)$ is the absorption coefficient at wavelength λ, $a_{CDOM}(\lambda_0)$ is the absorption coefficient at a reference wavelength λ_0 and S is the spectral slope in the spectral range from λ_0 to λ with $\lambda_0 < \lambda$.

Optics EXPRESS

Recent works have demonstrated the importance of the slope in the range of 275-295 nm ($S_{275\text{-}295}$) for better constraining the natural variability in the DOC specific absorption coefficient (a^*_{CDOM}) [25,26,32,33]. Furthermore, Helms et al. [32] highlighted the importance of the slope ratio $S_R = S_{275\text{-}295}/S_{350\text{-}400}$ as a potential proxy for assessing DOM molecular weight. Consequently, $S_{275\text{-}295}$, $S_{350\text{-}400}$ and the slope ratio S_R were specifically computed in this study.

2.2.2 pCO_2 and DOC

Water was collected for analysis using a Shurflo submersible pump with a 297 µm mesh at the surface. For the determination of pCO_2 the surface water samples were collected in triplicate (1 L) and stored in polycarbonate bottles closed with a silicone stopper equipped with two stop-cocks and short/long straws to allow creation of a headspace [49]. The bottles were filled with sample water, leaving no headspace. After injecting 60 mL of synthetic gas and removing 60 mL of water, the bottle was sealed and shaken vigorously for 2 min. The headspace was then removed with a 60-mL syringe and directly injected into a Picarro G2201-i Cavity Ring-Down Spectrometer (CRDS). pCO_2 values were corrected based on the common gas law.

DOC samples were collected in triplicate, and filtered through pre-combusted (500°C, 5 hours) GF/F glass fiber filters 0.7 µm nominal pore size (Whatman) and stored in 25 mL pre-combusted glass vials washed with acid, closed with Teflon lids and preserved in the field with 25 µL of 50% HCl at 0-4°C. DOC concentration (µmol L^{-1}) was measured using a Shimadzu total carbon analyzer (Model TOCVCPH). Only samples with a coefficient of variation lower than 10% among the triplicates were considered in this study. Measurements of DOC and $a_{CDOM}(412)$ were used to calculate the DOC specific coefficient absorption ($a^*_{CDOM}(412) = a_{CDOM}(412)/DOC$), expressed here in units of m^2 $mmol^{-1}$.

2.2.3 Chlorophyll-a concentrations and ancillary parameters

The chlorophyll-*a* concentration (chl-*a*) was measured on a Turner Designs Model 10 AU Fluorometer using triplicate samples filtered in the dark on 25 mm Whatman GF/F glass fiber filters (0.7 µm nominal pore size). Filters were wrapped in aluminum foil and frozen at –20°C in the field and subsequently frozen in liquid nitrogen. Prior to fluorometric analysis, pigments were extracted from the filters using a mixture of dimenthylsulfoxide: 90% acetone (2:3 ratio) for 24 h at 5°C and in the dark.

For each sampling station, the temperature of the surface water was recorded (Thermo Scientific Orion 4-Star instrument).

2.2.4 Statistics

The accuracy of [DOC], $a^*_{CDOM}(412)$, $S_{275\text{-}295}$ and pCO_2 estimates were evaluated using various statistical indicators including the root mean square error (RMSE), the mean relative absolute difference (MRAD) and the mean relative difference (Bias) expressed respectively as:

$$RMSE = \sqrt{\frac{\sum_{i=1}^{N}\left(y_i - x_i\right)^2}{N}} \tag{3}$$

$$MRAD = 100 \cdot \frac{1}{N}\sum_{i=1}^{N}\frac{\left|y_i - x_i\right|}{x_i} \tag{4}$$

$$Bias = 100 \cdot \frac{1}{N}\sum_{i=1}^{N}\frac{y_i - x_i}{x_i} \tag{5}$$

Optics EXPRESS

where x_i is the in situ data for a define parameter and y_i its estimated value.

3. Results and discussion

3.1 Optical and biogeochemical variability of the Lower Amazon River and tributary waters

Over the studied period, the average values for chl-*a* (1.3 ± 0.4 mg L^{-1}), DOC (306 ± 27 µmol L^{-1}), pCO_2 (2777 ± 1719 µatm) and temperature (29.8 ± 0.8 °C) recorded over the Lower Amazon River were in the range of observations previously reported in the region [7,8,14,39]. The average $a_{CDOM}(412)$ (m^{-1}) for the Amazon River during these cruises (3.6 ± 1.0 m^{-1}) was similar to the $a_{CDOM}(400)$ value (2.97 m^{-1}) reported for the Curuai floodplain [50] (Table 2).

Table 2. General statistics (maximum, minimum, mean, standard deviation – SD, and coefficient of variation - CV) for clearwater (CW) and Amazon River stations considering all sampling periods (2014-2017).

	CW			Amazon River		
	Average ± SD	CV %	Range	Average ± SD	CV %	Range
DOC (µmol L^{-1})	271 ± 103	40	134-503	306 ± 27	9	266-377
$a_{CDOM}(412)(m^{-1})$	3.3 ± 1.5	45	1.0-5.9	3.6 ± 1.0	28	2.5-7.0
$a^*_{CDOM}(412)$ (m^2.$mmol^{-1}$)	0.012 ± 0.004	34	0.005-0.019	0.012 ± 0.002	20	0.009-0.018
$S_{275-295}$ (nm^{-1})	0.015 ± 0.002	11	0.013-0.019	0.014 ± 0.0004	3	0.013-0.015
$S_{350-400}$ (nm^{-1})	0.017 ± 0.001	8	0.014-0.018	0.016 ± 0.001	4	0.015-0.018
Slope Ratio	0.91 ± 0.16	16	0.77-1.26	0.87 ± 0.03	3	0.80-0.94
pCO_2 (µatm)	2010 ± 1472	73	451-5030	2777 ± 1789	62	1045-6474
chl-*a* (mg L^{-1})	6.4 ± 7.6	118	1.7-31.3	1.29 ± 3.8	30	0.6-2.2
Temp (°C)	30.1 ± 0.7	2	28.9-31.6	29.8 ± 0.8	3	28.5-30.7

Amazon River samples had slightly lower temperature and chl-*a* values than the CW tributaries, with their higher primary production rates and lower turbidity [51] (Table 2). All parameters other than temperature generally presented a higher seasonal variability for the CW stations compared to the mainstream. Average $a_{CDOM}(412)$ values were similar between Amazon River and CW samples (3.6 vs 3.3 m^{-1} respectively). However, higher DOC and pCO_2 were observed in the Amazon River waters when compared to the other rivers. On the other hand, CW rivers generally had higher values of $S_{275-295}$ and S_R (0.015 nm^{-1} and 0.91, respectively, $p<0.01$) indicating differences in DOM quality between these different waters of the Amazon basin. The highest values for $S_{275-295}$ and S_R were found in CW tributaries when compared to those collected within the Amazon River (0.014 and 0.87 nm^{-1}, respectively), indicating the presence of lower molecular weight DOM that could be attributed to the higher abundance of algae [32]. These results are similar to molecular level differences in DOM composition previously observed in the Tapajós and Amazon rivers [52].

All parameters other than temperature generally presented a higher temporal variability for the CW stations, emphasizing the seasonal modulation in the intensity of the water mixing of the clear rivers and Amazon River according to the discharge season (Table 2).

Two different seasonal patterns regarding the DOM dynamics could be identified in the Amazon River. First, average CDOM and DOC values for samples corresponding to T1, T2, T3 and T5 cruises are following the discharge patterns with a clear co-variation between CDOM and DOC levels. The highest CDOM and DOC average values (Table 3, 4.6 and 4.7

m^{-1}, 297 and 337 µmol L^{-1} for CW and Amazon River, respectively) were found during high river discharges conditions (T1), while the lowest ones (Table 3, 2.8 m^{-1} and 287 µmol L^{-1} for the Amazon River) are occurring during low discharge conditions (T2 and T5), especially during T5 due to a severe drought in 2016 related to an El Niño event [20]. Intermediary values (Table 3, 2.6 and 4.2 m^{-1}, 171 and 313 µmol L^{-1} for CW and Amazon River, respectively) are found during transition period (falling conditions, T3). The latter pattern tends to suggest that the DOM concentration of the Lower Amazon region is mainly driven by the intensity of the river discharge and therefore the inputs from land-floodplains.

Table 3. Average of parameters (± standard deviation) for each sampling campaign for the clearwaters (CW) and Amazon River (Am) samples.

	T1 (High)		T2 (Low)		T3 (Falling)		T4 (Rising)		T5 (Low)	T6 (High)
	CW	Am	CW	Am	CW	Am	CW	Am	Am	Am
DOC (µmol L^{-1})	297 ± 72	337 ± 20	186 ± 41	303 ± 22	171 ± 22	313 ± 64	371 ± 80	381 ± 15	287 ± 12	420 ± 24
$a_{CDOM}(412)$ (m^{-1})	4.6 ± 0.3	4.7 ± 1.1	1.7 ± 1.0	3.3 ± 0.7	2.6 ± 0.7	4.2 ± 0.4	3.9 ± 1.3	3.6 ± 0.3	2.8 ± 0.3	3.3 ± 0.1
$a^*_{CDOM}(412)$ ($m^2.mmol^{-1}$)	0.016 ± 0.0028	0.014 ± 0.0023	0.010 ± 0.0051	0.011 ± 0.0017	0.015 ± 0.0023	0.014 ± 0.003	0.010 ± 0.0022	0.009 ± 0.0005	0.010 ± 0.0007	0.008 ± 0.0005
$S_{275-295}$ (nm^{-1})	0.014 ± 0.0006	0.014 ± 0.0004	0.017 ± 0.0019	0.014 ± 0.0006	0.015 ± 0.0011	0.014 ± 0.0003	0.014 ± 0.0007	0.014 ± 0.0003	0.015 ± 0.003	0.015 ± 0.0002
$S_{350-400}$ (nm^{-1})	0.016 ± 0.0004	0.016 ± 0.0005	0.015 ± 0.0007	0.016 ± 0.001	0.017 ± 0.0001	0.017 ± 0.0003	0.018 ± 0.0005	0.017 ± 0.0004	0.017 ± 0.0003	0.018 ± 0.0001
Slope Ratio	0.85 ± 0.01	0.86 ± 0.01	1.18 ± 0.08	0.89 ± 0.04	0.87 ± 0.06	0.85 ± 0.02	0.81 ± 0.04	0.82 ± 0.02	0.88 ± 0.02	0.82 ± 0.01
pCO_2 (ppm)	3345 ± 1685	4779 ± 1060	853 ± 529	1590 ± 458	2104 ± 1486	3981 ± 1414	2115 ± 1213	1888 ± 495	1146 ± 93	———
chl-*a* (mg L^{-1})	17.1 ± 14.2	1.0 ± 0.2	6.2 ± 2.0	1.7 ± 0.3	2.4 ± 0.5	0.8 ± 0.2	4.7 ± 2.8	1.4 ± 0.4	1.4 ± 0.1	———
Temp (°C)	29.7 ± 0.05	28.8 ± 0.2	30.8 ± 0.6	30.3 ± 0.3	29.4 ± 0.4	29.0 ± 0.2	30.3 ± 0.4	30.1 ± 0.6	30.3 ± 0.5	———
Discharge (m^3/s)	284100 ± 2769		117785 ± 835		265028 ± 1731		205013 ± 965		98237 ± 164	269048 ± 451

Specific situations departing from such general seasonal modulations were, however, observed during T4 and T6. For these two cruises $a_{CDOM}(412)$ values remained relatively low (3.6 and 3.3 m^{-1}, respectively), when compared to the corresponding DOC contents (381 and 420 µmol L^{-1}), leading for these two cruises to the lowest $a^*_{CDOM}(412)$ average values (0.009 and 0.008 $m^2.mmol^{-1}$, for T4 and T6, respectively Table 3). The patterns observed for T4 and

T6 tend to indicate that the terrestrial inputs of DOC and CDOM to the Lower Amazon are not fully co-varying with the river discharge. As a matter of fact, the correlation between DOC average values and the discharge data are much higher when excluding rising condition measurements (R^2 = 0.16 considering all the cruises and 0.79 excluding T4 and T6, data not shown), with relatively high DOC contents with respect to the corresponding Amazon discharge levels for these two cruises (Table 3).

The latter peculiar feature tends to indicate the presence of strong seasonal modulation in the DOM quality according to the timing of discharge and not only its intensity. T4 is corresponding to the rising season. In this case, the low CDOM-high DOC situation might reflect a difference in the quality (lability) of the DOM accumulated in source areas (e.g. floodplains, flooded forest, seasonally isolated lakes [11],) and then mobilized during the increase of the Amazon waters level. The situation for the T6 samples (April 2017 beginning of the high season) is globally similar to the one found during T4 (February 2016). During the year of 2017 a modification occurs in the general river discharge pattern, probably linked to the El Niño event of 2015-2016 [18,20], as illustrated here by the decay of about one month in the maximal discharge values recorded at Óbidos in 2017 (beginning of May), when compared to the situations observed from 2014 to 2016 (late May, Fig. 1). This suggests that besides seasonal modulation, inter-annual variability in the timing of the hygrometric regime can modulate the quality of the DOM mobilized from land-floodplain flush and delivered to the river. Note that short time scale processes such as strong rain event might also represent another source of variability in the quality of the terrestrial DOM inputs, as emphasized in other tropical environments [53]. Temporal variability in the average $S_{275\text{-}295}$ and S_R are relatively narrow when compared to the variability found at spatial scale between the different water types (CW, Amazon) investigated in the frame of this study (Tables 2 and 3). The slightly lowest S_R values found for T4, T6 might suggest the presence of DOM with a higher molecular weight for these two cruises when compared to the other cruises. However, the understanding of the source and sink mechanisms driving this apparent heterogeneity in the DOM characteristics of the Lower Amazon according to the discharge conditions (intensity and timing), would require additional measurements including some specifically dedicated to the characterization of the seasonal DOM dynamics within the diversity of source areas surrounding the Lower Amazon.

The latter temporal patterns were not observed for the pCO_2 values. An ANOVA of pCO_2 between different seasons, combined with a post-hoc test (Tukey HSD for unequal N), reveals that pCO_2 for the stations of the Amazon was higher during the high (T1) and falling (T3) seasons while the data for the other cruises showed the same mean values ($p > 0.05$). In contrast with the Amazon samples, no clear seasonal pattern can be found regarding the biogeochemical and bio-optical properties of the CW samples. This might be related to the higher complexity of the factors driving DOM dynamics for the corresponding water masses which result for the balanced effects of autochthonous and allochthonous DOM inputs, mixing processes between CW and Amazon River waters and modulation related to both bacterial and photochemical degradation processes. Low CDOM and DOC values are found during the Low and Falling seasons (T2 and T3, respectively) translating the combined action of low allochthonous (low land flush) and autochthonous (low chl-*a*) sources of DOM. As observed for the Amazon River, high DOC values recorded for CW during T4 were not associated with an equivalent raise in the CDOM values reinforcing the peculiar characteristics of the DOM input during the rising season. No seasonal difference was found in the pCO_2 recorded for the CW samples ($p > 0.05$).

In order to illustrate the spatial variability from the Lower Amazon to the river's mouth, average $a_{CDOM}(412)$, [DOC], $pCO2$, $a^*_{CDOM}(412)$, S_R and $S_{275\text{-}295}$ are represented for each cruise in Fig. 2. The spatial distribution show that the carbon content (DOC: Fig. 2(a) and pCO_2 Fig. 2(c)) generally decreased from Óbidos to the river mouth. This general pattern remained consistent for all the seasons sampled, except for DOC during the falling season

Optics EXPRESS

(T3), which tended to increase towards the mouth of the river (Macapá), while no similar pattern could be observed for CDOM. The increase of DOC along the transect Óbidos-Macapá was reported by Ward et al. [8] as a result of the combination of strong organic matter inputs from tributaries and floodplains and the degradation of particulate carbon into dissolved molecules. Such high export rates of labile organic matter from floodplains to the river during the falling season, was also reported by Moreira-Turcq et al. [14]. However, this labile material does not persist further out into the plume once exported to the ocean, leaving behind a background of recalcitrant DOM [54,55].

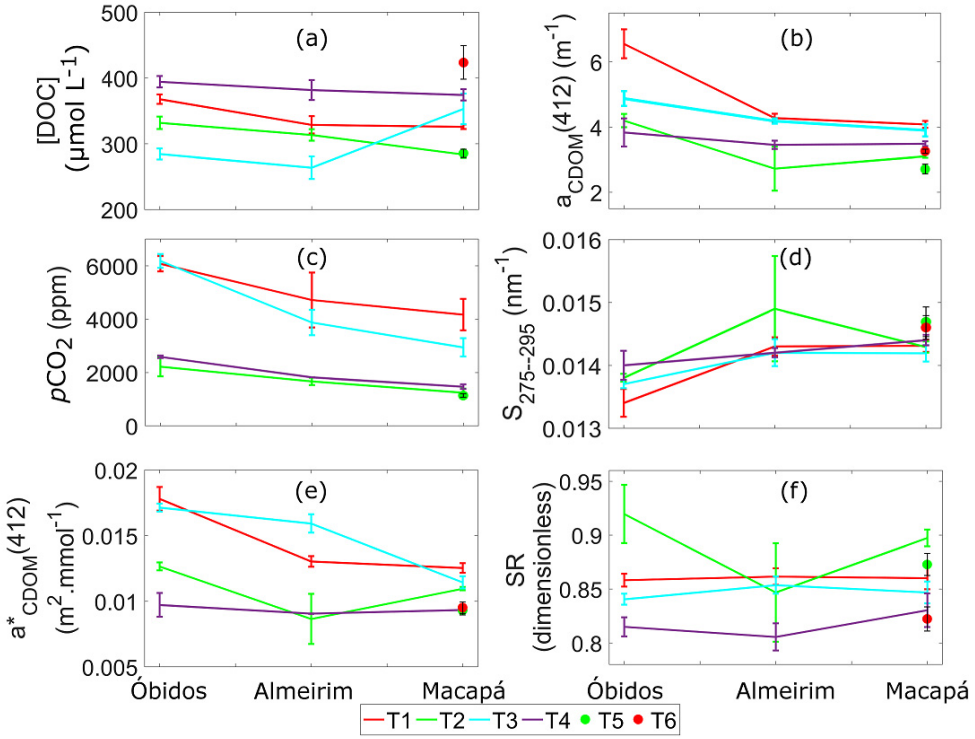

Fig. 2. Spatial distribution of biogeochemical parameters along the Amazon mainstream. The parameters were averaged for each station per season. The first station is at Óbidos (~900 km from the mouth). The middle of the transect is at Almeirim (~450 km from the mouth). The transect ends at the Amazon mouth, in Macapá, and T5 and T6 were sampled at the river mouth only.

As observed for DOC, CDOM values show a general decreasing gradient from the Lower Amazon to the river mouth (Fig. 2(b)) highlighting the impact of DOM degradation processes (especially bacterial) along the river course, as reported by other studies [23,56]. This feature is confirmed here, by the increasing gradient generally found for $S_{275\text{-}295}$, with Fig. 2(d) suggesting a gradual decrease in DOM molecular weight (Fig. 2(d)) from Óbidos to Macapá. Interestingly, such changes in the DOM quality within the Amazon River is also illustrated here by the general sharp decreasing patterns in $a^*_{CDOM}(412)$, translating differences in the intensity of the degradation rates for DOC and CDOM along the Amazon water course (Fig. 2(e)).

Note that CDOM, DOC and pCO_2 spatial distribution showed a slight inflexion point at Almeirim (Fig. 2), emphasizing a potential influence of inputs of the CW from the Paru River on the optical and biogeochemical characteristics of this area [56] (Table 2). The decrease in the CO_2 degassing along the Lower Amazon River region reported here, is consistent with previous observations provided by Sawakuchi et al. [7].

Optics EXPRESS

3.2 $a_{CDOM}(412)$ to DOC relationships

Considering the whole data set gathered in the frame of this study, the direct relationship between $a_{CDOM}(412)$ and DOC (N = 80; R^2 = 0.17, p<0.05) had a low accuracy (Fig. 3(a)). This absence of general co-variation between CDOM and DOC can be related to two specific features.

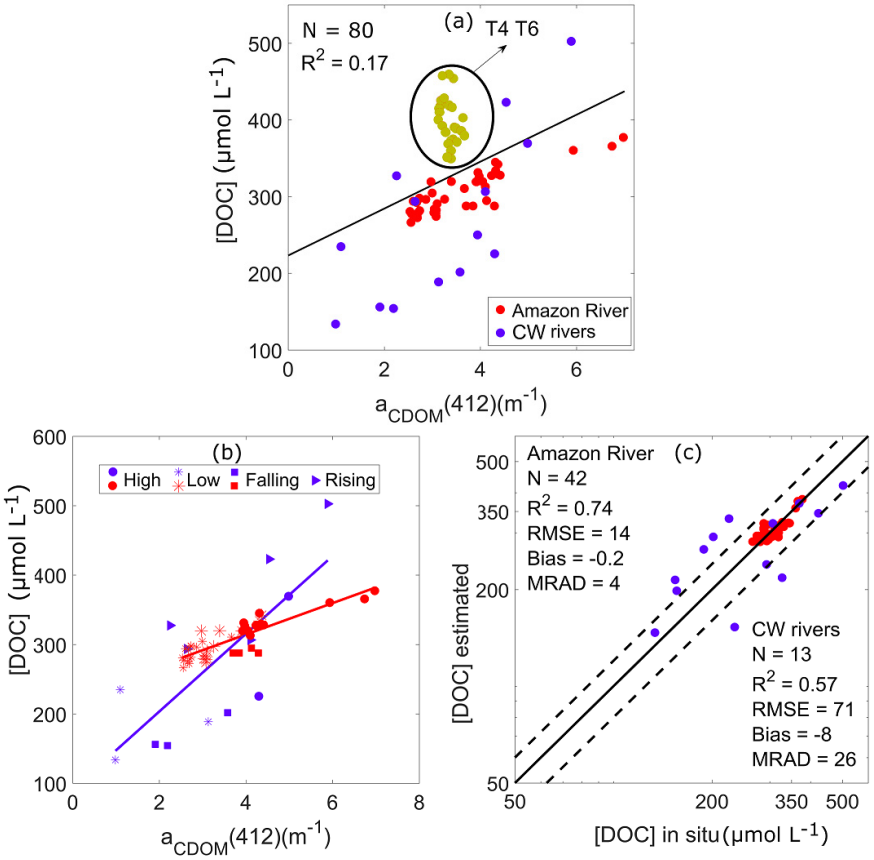

Fig. 3. a) Direct relationship between $a_{CDOM}(412)$ and [DOC] for: a) All data from the Lower Amazon (N = 80; R^2 = 0.17, p<0.05); b) Amazon River (T1-T3, T5), (N = 42, R^2 = 0.74, p<0.05) and CW rivers (N = 13, R^2 = 0.57, p<0.05); c) Scatter plot of estimated [DOC] as a function of the direct relationship of in situ [DOC] and $a_{CDOM}(412)$ (Amazon River: N = 42, R^2 = 0.74, RMSE = 14, Bias = –0.2; MRAD = 4; CW rivers: N = 13, R^2 = 0.57, RMSE = 71, Bias = –8; MRAD = 26). Data from T4 and T6 (N = 25) are not showed in a separated panel due the absence of significant direct CDOM-DOC relationship. Solid lines represent 1:1 line and dashed lines represent the 20% error lines.

First, Amazon River water samples for T4 and T6 present a pattern very different from the other cruises, with a general decoupling between CDOM and DOC data (Fig. 3(a)). This absence of co-variation between CDOM and DOC for T4 and T6 can be related to the peculiar characteristics of the terrestrial DOM inputs induced by land-floodplain flush during the rising of the Amazon waters. Here, the decoupling observed between CDOM and DOC could translate a spatial heterogeneity in the DOM sources mobilized during such discharge conditions. Floodplain areas surrounding the Amazon have been for instance showed to be extremely heterogeneous in terms of vegetation-water connections [11,18]. However, no information about the DOM dynamics in the latter water bodies is currently available.

Optics EXPRESS

Second, a clear discrepancy in the link between CDOM and DOC exists when considering the CW (whole data set) and Amazon samples (for T1, T3 and T5) separately (Fig. 3(a)). When splitting these data (Fig. 3(b)), two different significant linear relationships between $a_{CDOM}(412)$ and DOC can be drawn (Fig. Fig. 3(c), Amazon River: N = 42, $R^2 = 0.74$, $p<0.05$; CW: N = 13, $R^2 = 0.57$, $p<0.05$) underlining the strong biogeochemical heterogeneity of the Amazon basin water masses. The dispersion around these two relationships can be partly attributed to seasonal modulation in DOM quality; however, more data are needed to clarify the impact of these seasonal patterns, especially for the CW data set which is relatively small (N = 13). Note that the presence of such linear dependency between CDOM and DOC is not due, unlike coastal waters, to mixing processes, but more likely to a parallel (biological and photochemical) degradation of both CDOM and DOC along the Amazon River course.

The differences in the slope and offset values for the CDOM to DOC relationships derived for the Amazon and CW samples (22.6 and 224 µmol L^{-1}, 54 and 91.3 µmol L^{-1}, respectively) suggest differences regarding the source and sink factors acting on DOM dynamics in these two optically different water types of the Amazon basin. The higher average $S_{275-295}$ and S_R for the CW samples (Table 2) tend to indicate the presence of DOM of lower molecular weight than for the Amazon samples. Such differences might be attributed to variation in the DOM origin as larger contribution of the phytoplankton derived DOM in CW [8] as well as variation in the intensity of the photo-degradation processes (greater in the less turbid and more stagnating CW samples of the Xingu and Tapajos rivers).

These results suggest that the estimation of DOC from CDOM absorption coefficient using a simple linear model might be possible taking into account specific information about the optical water type, and thus biogeochemical quality (Fig. 3(b), (c)). This might be achieved using optical classification based approaches whose advantages have been demonstrated for diverse applications dealing with the estimation of various biogeochemical products from ocean colour remote sensing (e.g [57–59].). However, our results also emphasize that such direct CDOM to DOC models are invalid and would result in inaccurate estimations of DOC (e.g. T4: rising conditions, T6: shift in the discharge timing).

Several studies have emphasized the use of spectral slope $S_{275-295}$ for assessing a^*_{CDOM} and thus better constraining the natural variability in the dependency between CDOM and DOC at both seasonal [33] and regional [25,34] scales. The interest of using $S_{275-295}$ for estimating DOC from CDOM was also evaluated in the frame of this study. As previously observed for the direct CDOM-DOC relationship, a low correlation between $a^*_{CDOM}(412)$ and $S_{275-295}$ is observed when our whole data set is considered (N = 80; $R^2 = 0.26$, $p<0.05$). When excluding the peculiar samples corresponding to T4, T6, a significant nonlinear relationship can however be drawn between $a^*_{CDOM}(412)$ and $S_{275-295}$ for T1 to T3 and T5 considering both Amazon and CW samples (Fig. 4(a)).

Optics EXPRESS

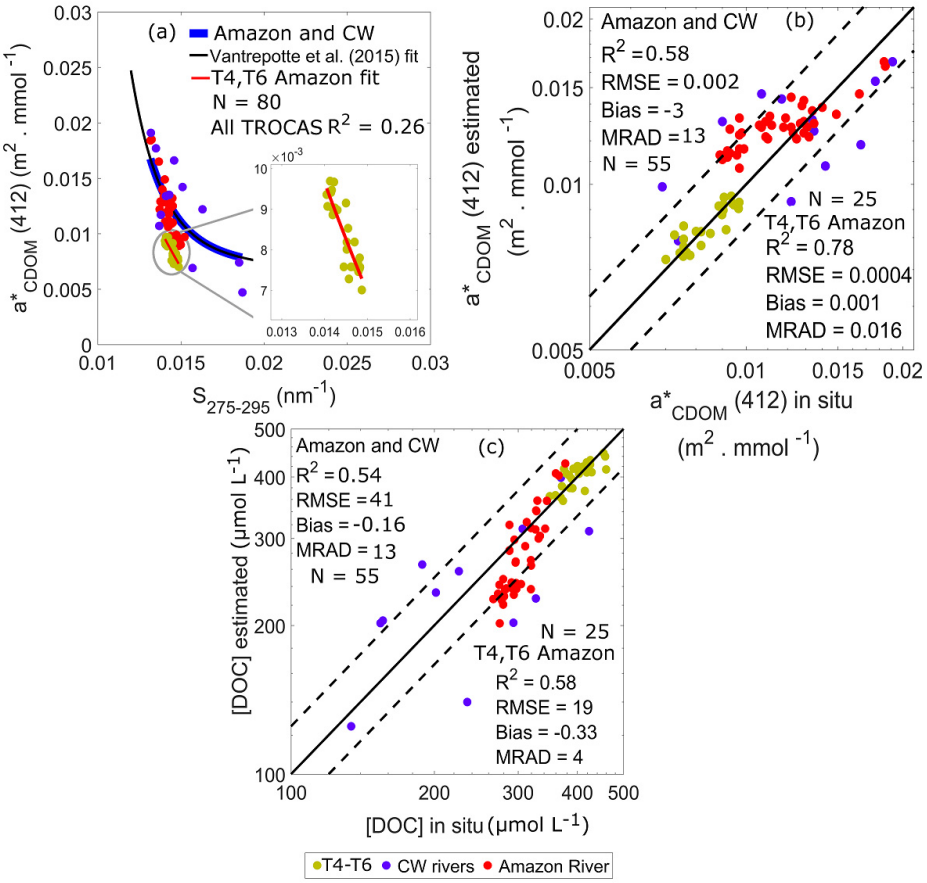

Fig. 4. a) Relationship between $S_{275\text{-}295}$ and $a^*_{CDOM}(412)$ for Amazon River (T1-T3, T5), clearwater rivers and T4, T6 Amazon samples (N = 80, R^2 = 0.26, $p<0.05$), and zoom for the relationship between $a_{CDOM}(412)$ and $S_{275\text{-}295}$ for T4, T6 Amazon samples (N = 25), Vantrepotte et al. [25] fit for comparison; b) Estimated $a^*_{CDOM}(412)$ ($S_{275\text{-}295}$ method) as a function of the measured $a^*_{CDOM}(412)$ for Amazon + clearwater rivers (N = 55, R^2 = 0.58, $p<0.05$, RMSE = 0.002, Bias = –3; MRAD = 13), and for T4, T6 Amazon samples (N = 25, R^2 = 0.78, $p<0.05$, RMSE = 0.0004, Bias = 0.001; MRAD = 0.016) in log10 scale; c) Estimated [DOC] as a function of the $a^*_{CDOM}(412)$ and $S_{275\text{-}295}$ for Amazon + clearwater rivers (N = 55, R^2 = 0.54, $p<0.05$, RMSE = 41, Bias = 0.16; MRAD = 13), and for T4, T6 Amazon samples (N = 25, R^2 = 0.58, $p<0.05$, RMSE = 19, Bias = –0.33; MRAD = 4) in log10 scale. Solid lines represent 1:1 line and dashed lines represents the 20% error lines.

This non-linear model is very close to the one proposed by Vantrepotte et al. [25], from a large data set gathering data collected within highly contrasting coastal waters dominated by terrestrial inputs of DOM. Further, the general validity of this model, when considering the data of Amazon River (T1-T3, T5) and CW rivers, emphasizes the interest of such $S_{275\text{-}295}$ based approach for avoiding issues related to the use of water masses information as suggested for direct CDOM to DOC linear models. It is worth noting, however, that such a $S_{275\text{-}295}$ based model might induce a decrease of performance in the DOC retrieval when compared to direct CDOM-DOC relationships, as observed here especially for the samples collected during low water conditions (relative errors reaching 20%, Fig. 4(c)). Our results further indicate that a unique $S_{275\text{-}295}$ vs $a^*_{CDOM}(412)$ model is not sufficient to take into account the occurrence of very specific conditions such as the ones identified for the samples collected during T4 and T6, for which a specific model is required (Fig. 4(a)).

Note that a significant relationship between $S_{275-295}$ vs $a^*_{CDOM}(412)$ was found for these samples (N = 25, R^2 = 0.78, $p<0.05$, RMSE = 0.0004, Bias = 0.001, MRAD = 0.016) (Fig. 4(b)) whereas a general scattering was conversely observed when looking to the direct link between CDOM and DOC for the corresponding data (Fig. 3(b)). The better result for T4, T6 in comparison to Amazon and CW (R^2 = 78 and R^2 = 58, respectively, Fig. 4(b)) can be explained by the data set of similar bio-optical characteristics. Amazon and CW gather samples from contrasted turbidity while T4 and T6 where sampled only on Amazon waters with similar optical constituents.

Interestingly, a sharp non-linear relationship was found between $a_{CDOM}(412)$ and $S_{275-295}$ (Fig. 5) as reported by other authors [25]. This unique relationship derived from our whole data set indicates the link between CDOM quality and quantity, and suggests the possible assessment of $S_{275-295}$ from $a_{CDOM}(412)$ for remote sensing applications.

The expressions and coefficients used to develop the relationship of CDOM-DOC are documented in Table 4.

Table 4. Expressions and coefficients for the relationship $a^*_{CDOM}(412)$ vs $S_{275-295}$, $S_{275-295}$ vs $a_{CDOM}(412)$ and $a_{CDOM}(412)$ vs DOC (Am – Amazon samples; CW – clearwater samples).

	Coefficients and R^2				
Expression	General (Am + CW + T4,T6)	General (Am + CW)	Regional Am	Regional CW	Regional T4,T6
$a^*_{CDOM}(412) = a \cdot \left(e^{(b \cdot S_{275-295})} - e^{(c \cdot S_{275-295})}\right) + d$ (Fig. 4)	a = –6.99	a = 6.00	—	—	a = 2.974
	b = –54.4	b = –60.93	—	—	b = –38.83
	c = –63.4	c = –53.27	—	—	c = –35.46
	d = 0.40	d = 0.30	—	—	d = 0.09
	R^2 = 0.26	R^2 = 0.58	—	—	R^2 = 0.78
$S_{275-295} = \frac{\left(a + b \cdot \left(a_{CDOM}(412)\right)\right)}{\left(c + d \cdot \left(a_{CDOM}(412)\right)\right)}$ (Fig. 5)	a = 0.0425	—	—	—	—
	b = 0.1061	—	—	—	—
	c = 1	—	—	—	—
	d = 9.238	—	—	—	—
	R^2 = 0.85	—	—	—	—
$DOC = a \cdot a_{CDOM} + b$ (Fig. 3)	a = 30.59	a = 32.59	a = 22.61	a = 54.64	a = –69.76
	b = 223.2	b = 176.48	b = 223.9	b = 96.56	b = 635.8
	R^2 = 0.17	R^2 = 0.51	R^2 = 0.74	R^2 = 0.57	R^2 = 0.14

Optics EXPRESS

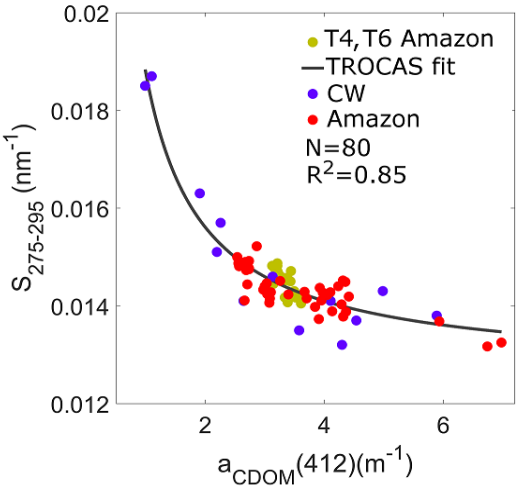

Fig. 5. Relationship between $a_{CDOM}(412)$ and $S_{275-295}$ for all sampling campaigns (N = 80, R^2 = 0.85, p<0.05).

3.3 $a_{CDOM}(412)$ and pCO_2 relationship

Various studies have documented significant relationships between pCO_2 and DOC in boreal and temperate inland waters [36–38]. Based on results from this study, we have not observed such a link between pCO_2 and DOC in the Lower Amazon River waters (N = 69, R^2 = 0.04, p>0.05, Fig. 6(a)). This result is consistent with other studies in tropical inland waters [39,40,60], also emphasizing an absence of correlation between these two parameters in various Brazilian lakes, including some located in the Amazon basin. Rather, the pCO_2 has been related to rainfall and temperature [40,60,61]. In contrast, a strong linear positive relationship was found here between $a_{CDOM}(412)$ and pCO_2 (Fig. 6(b) and 7(a), (pCO_2 = 1240 * $a_{CDOM}(412)$ −1845, N = 69, R^2 = 0.65, RMSE = 979, p<0.05). This general relationship between $a_{CDOM}(412)$ and pCO_2 seems to be less affected by the optical water type or river discharge conditions, when compared to the results previously obtained regarding CDOM to DOC relationship.

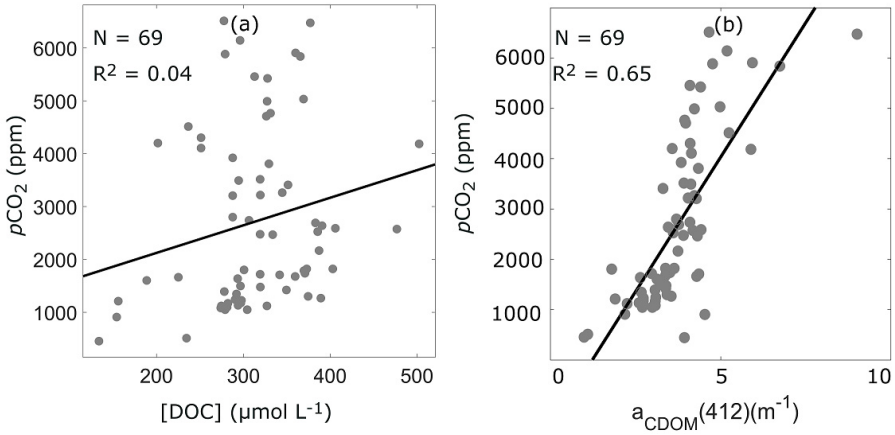

Fig. 6. a) DOC-pCO_2 linear relationship (N = 69, R^2 = 0.04, p>0.05) and; b) $a_{CDOM}(412)$-pCO_2 linear relationship (N = 69, R^2 = 0.65, p<0.05) in the Lower Amazon region.

Optics EXPRESS

Several studies have demonstrated the use of chl-*a* and surface temperature data (T) as a predictor for pCO_2 in diverse river-dominated coastal areas [62,63]. CDOM has also been used in combination with the aforementioned parameters as a proxy for salinity or humic substances [42,64,65]. The chl-*a* measurement indicates the presence of phytoplankton and therefore primary production that fixes CO_2, leading to lower values of pCO_2 [66]. Inversely, higher temperatures decrease the solubility of CO_2 [67] and DOM availability enhances bacterial respiration leading to higher pCO_2 [7,9,60,68].

Individual regressions (Table 5) indicate that degassing fluxes related to CDOM-degradation processes are the main factor driving pCO_2 dynamics in the Lower Amazon explaining 65% of pCO_2 variability through a linear relationship (Fig. 7(a)). Conversely, temperature and chl-*a* explain 49% and 30% of pCO_2 variability, respectively, and pCO_2 exhibit a non-linear dependency with the latter two parameters (Table 5).

Table 5. Simple regression models describing the relationship of pCO_2 and CDOM, temperature (T) and chl-*a* at the Lower Amazon.

Model	pco_2 =	R^2	RMSE	N
1	$1240 \cdot a_{CDOM}(412) - 1845$	0.65	979	69
2	$1.48 \cdot 10^{30} \cdot T^{-18.2}$	0.49	1200	69
3	$3180 \cdot chla^{-0.68}$	0.3	1411	69

The value added when including these two additional descriptors for estimating pCO_2 was specifically assessed using polynomial multivariate regression considering $a_{CDOM}(412)$, T and chl-*a* as descriptive variables. Results indicate that the inclusion of both CDOM and temperature provide better pCO_2 estimates (N = 69; R^2 = 0.80; RMSE = 757 ppm, Bias = –13, MRAD = 26) than a model based on CDOM and chl-*a* (N = 69; R^2 = 0.72; RMSE = 875 ppm, Bias = –11%, MRAD = 32%). A chl-*a* and temperature based model provides the lower pCO_2 retrieval accuracy (N = 69; R^2 = 0.54; RMSE = 1136 ppm, Bias = –16%, MRAD = 39%). Further, the consideration of CDOM, T and chl-*a* only slightly improve pCO_2 retrieval (N = 69; R^2 = 0.83; RMSE = 749 ppm, data not shown) when compared to the CDOM and T based model (Fig. 7(b)).

Optics EXPRESS

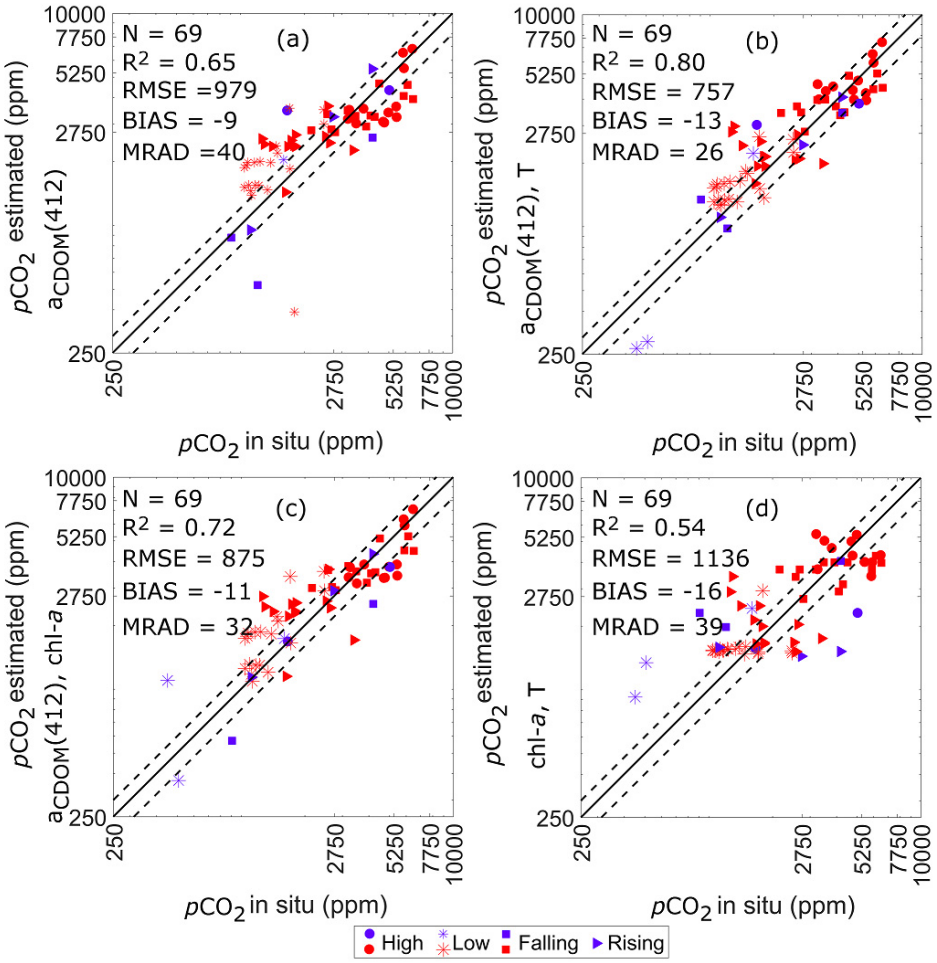

Fig. 7. Estimative of pCO_2 for different sampling seasons, clearwater and Amazon River: a) Estimated pCO_2 as a function of the $a_{CDOM}(412)$ (N = 69, R^2 = 0.65, p<0.05, RMSE = 979 ppm, Bias = –9, MRAD = 40, pCO_2 = 1240 * $a_{CDOM}(412)$ –1845); b) Estimated pCO_2 as a function of $a_{CDOM}(412)$ and temperature (N = 69, R^2 = 0.80, RMSE = 757 ppm, Bias = –13, MRAD = 26); c) Estimated pCO_2 as a function of $a_{CDOM}(412)$ and chl-*a* (N = 69, R^2 = 0.72, RMSE = 875 ppm, Bias = –11, MRAD = 32); d) Estimated pCO_2 as a function of temperature and chl-*a* (N = 69, R^2 = 0.54, RMSE = 1136 ppm, Bias = –16, MRAD = 39). All the figures are in log10 scale. Solid lines represent 1:1 line and dashed lines represent the 20% error lines.

The estimation of chl-*a* concentration from ocean colour remote sensing in very turbid waters such as those of the Amazon River remains very challenging [69,70]. The performance of models based on reflectance bands more suitable to retrieve chl-*a* in turbid environments (i.e. red and near infra-red) has been shown to provide a relevant alternative at least when chl-*a* concentration is sufficiently high (> 2mg m^{-3}) [70–73]. Such chl-*a* levels were never reached in this data set, with Amazon River samples showing an average chl-*a* concentration of 1.29 ± 0.38 mg m^{-3} (Table 2). Conversely, various studies have emphasized the possibility of using remotely-sensed temperature estimations in inland waters with a relatively high accuracy [74–77]. Considering these issues, a formulation based on CDOM and T for estimating pCO_2 in the Lower Amazon region could be developed:

$$pCO_2 = a\cdot\left(a_{CDOM}\left(412\right)^2\right)+b\cdot a_{CDOM}\left(412\right)+c+d\cdot\left(T^2\right)+e\cdot T+f\cdot\left(a_{CDOM}\left(412\right)\cdot T\right) \quad (6)$$

where T and $a_{CDOM}(412)$ represents the in situ river surface temperature and CDOM absorption coefficient, with the equation coefficients equivalent to: a = 49.24, b = 3001, c = 4.828 x 10^5, d = 526.6, e = –3.19 x 10^4, f = –83.52.

Similarly, various CDOM absorption inversion algorithms adapted to coastal or freshwaters environments have been also recently documented (e.g [78].). Considering the latter feature, a formulation based on CDOM and T for estimating pCO_2 in the Amazon waters is here proposed for assessing pCO_2 content, potentially applicable for further applications of ocean colour remote sensing.

Interestingly, in contrast with the previous results on DOC, these results suggest that a unique relationship can be used without distinguishing Amazon and CW data, or considering specific rain conditions (T4, T6), highlighting a greater stability in the factors driving CO_2 production, consumption, and outgassing.

4. Conclusions

The major aim of this study was to assess the potential use of $a_{CDOM}(412)$ for estimating DOC and pCO_2 content within the poorly-investigated region of the Lower Amazon River. To achieve the main goal, the spatial-seasonal variability was documented for the study period.

The heterogeneity of the DOM dynamics between clear and turbid water bodies of the Lower Amazon River region was clearly observed. The prevalent impact of degradation processes more likely related to bacterial activity has been further highlighted by the changing optical properties of CDOM along the course of the Amazon River that agree well with past observations of more degraded DOM molecular composition towards the river's mouth. Besides these general spatial features, a strong seasonal variability was found for both CDOM and DOC values. While the seasonality in the Amazon River discharge represents a major controlling factor for the DOM annual variation, results also illustrate the complexity of the DOM temporal dynamics in the Lower Amazon. Significant modulations in the DOM quality were specifically observed according to the discharge timing at either seasonal (rising conditions) or inter-annual (El Niño event) scales. The understanding of the CDOM and DOC dynamics depicted here in the Amazon mainstream would however need additional information specifically regarding the seasonal variation in the quality of DOM inputs, considering the diverse source areas surrounding the Lower Amazon (floodplains, flooded forest, seasonally isolated lakes).

The potential for the assessment of DOC loads from a CDOM inversion algorithm was investigated. Results demonstrate the strong heterogeneity of the water masses of the Lower Amazon region with its clear and turbid waters, suggesting that assuming a single direct CDOM to DOC relationship is problematic. While the use of $S_{275\text{-}295}$ based approach has been shown to represent a relevant alternative for assessing DOC from CDOM in coastal waters, results here tend to indicate that such optical proxy can only partly describe the natural variability of the CDOM to DOC ratio in the inner Amazon. A single $S_{275\text{-}295}$ based model is not able to capture the impact of DOM inputs potentially related to the seasonal modulation in the quality of the DOM delivered to the river from land–floodplain flush.

Finally, our results have demonstrated that CDOM absorption can be considered as a relevant proxy of the pCO_2 in the Lower Amazon. A model based on CDOM and temperature seems to provide the most reliable pCO_2 estimates (relative error of 26% on average). The assessment of the CO_2 flux from the entire Amazon River, including the lower reaches that are tidal-influenced, is crucial to understand the role of inland waters to the carbon budget. For example, past global estimates of CO_2 emissions do not include tidal rivers, and including the tidal reaches of the Amazon River, alone, increase global CO_2 outgassing estimates by ~43% [7]. Widely applying the optical approach used here will allow a broader assessment of the lower reaches of rivers worldwide and allow for more persistent monitoring of alterations to aquatic carbon cycling under a changing climate.

Optics EXPRESS

Funding

Fundação de Amparo à Pesquisa do São Paulo (FAPESP) (12/51187-0); National Science Foundation (NSF) (1256724); Coordenação de Aperfeiçoamento de Pessoal de Nível Superior (CAPES) (33010013005P0).

Acknowledgments

The authors would like to thank Daimio Brito and Gilvan Portela de Oliveira for the laboratory and logistical support in Macapá (Laboratory of Chemistry, Sanitation and Modeling Environmental Systems – LQSMSA/UNIFAP. Cica and the crew of the B/M Mirage for the contributions during the river cruises. The Center for Nuclear Energy in Agriculture Laboratory (CENA/USP) and Laboratory of Aerosols, Aqueous Solutions and Technologies (LAQUATEC/INPE) for the analysis of the samples.